

# Effect of ion entry acceptance conditions on the performance of a quadrupole mass spectrometer operated in upper and lower stability regions

P. Turner<sup>a)</sup>

Department of Electrical Engineering and Electronics, Liverpool University, Brownlow Hill, Liverpool L69 3BX, United Kingdom  
and Sira Technology, Ltd, South Hill, Chislehurst, Kent BR7 5EH, United Kingdom

S. Taylor and J. R. Gibson

Department of Electrical Engineering and Electronics, Liverpool University, Brownlow Hill, Liverpool L69 3BX, United Kingdom

(Received 18 June 2004; accepted 14 February 2005; published 21 April 2005)

Computer simulation of ion motion in a quadrupole mass spectrometer has been used to examine the effect of initial ion conditions on performance when operated in the first and third zones of the Mathieu stability diagram. Commercial instruments frequently use round electrodes instead of the better-performing hyperbolic electrodes because the cost of manufacturing is lower. However, adverse features are seen when using round electrodes. Here further insight is provided and a possible method of correction is suggested. For the first time, ion origin for the first stability region for a round electrode quadrupole has been reported. © 2005 American Vacuum Society. [DOI: 10.1116/1.1894665]

## I. INTRODUCTION

Quadrupole mass analyzers separate ions according to their mass-to-charge ( $m/z$ ) ratios. The quadrupole analyzer consists of four parallel conducting electrodes, with opposing rods electrically connected: One pair at  $+U$  volts, and the second at  $-U$  volts. A radio-frequency (rf) signal ( $+V \cos \omega t$ ) is applied to the first pair of rods, and a signal retarded by  $180^\circ$  is applied to the second pair ( $-V \cos \omega t$ ).

The  $xy$  plane provides a cross section of the quadrupole (Fig. 1). The ions can proceed down the analyzer perpendicular to this plane ( $z$  axis). Ions have a transverse motion in the  $x$  and  $y$  planes. The oscillating field selectively accelerates ions to and from the electrodes. Controlling the  $U:V$  ratio establishes fields such that ions of one  $m/z$  ratio are able to pass down the entire length of the analyzer.<sup>1</sup>

Modern computer models allow the computation of large numbers of ions and their trajectories through the mass analyzer. The work here uses the model described by Gibson *et al.*<sup>2</sup> Computer simulations have been used to investigate  $r/r_0$  optimum values,  $r$  is the electrode radius and  $r_0$  defines rod separation as in Fig. 1. The application of a static magnetic field to the analyzer and the effect of electrode size<sup>3-6</sup>

The program generates ions uniformly across a disc centered on the quadrupole axis; ions have equal energy and no beam spread, variation in these parameters can be attributed to the ion source design, ideal conditions have been assumed. The initial parameters of the successful ions, the  $x$ - $y$  position, velocity and phase angle at point of entry are stored for later analysis. The quadrupole fields are assumed to start as soon as the ions leave the source. Thus fringe fields between

the source and quadrupole rods are ignored. Successful ions are considered to be those reaching the detector defined by the exit aperture. The ions are considered to travel freely at a constant velocity in the  $z$  direction because fringing fields are ignored. If the amplitude of the ion's trajectory equals or exceeds the radius  $r_0$ , the ion is considered to be unsuccessful (rejected from the analyzer). Figure 1 shows the quadrupole rod system defining the  $X$  and  $Y$  regions in relation to the alignment of the rods and the applied voltages.

Ions enter the quadrupole at random values of the rf phase. Within the model, the trajectory of the ion is divided into segments, and motion over the segment is computed by consideration of the local fields. The description of ion motion is approximated using the fourth-order Runge-Kutta differential equation.

Figure 2 shows the Mathieu stability diagrams. There are a number of regions in which the ion motion is stable in both the  $x$  and  $y$  planes. The stability diagrams define parameters  $a$  and  $q$  which correspond to the regions of stability in the  $x$  and  $y$  planes. The  $a$  and  $q$  parameters are defined by

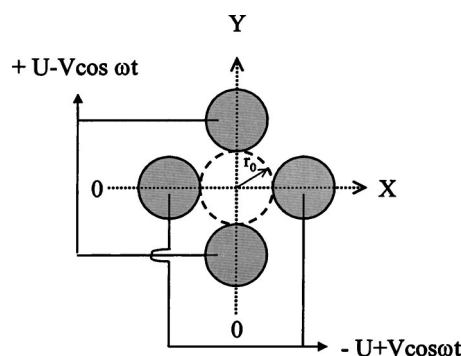


FIG. 1. Rod positions in relation to  $x$  and  $y$  axes for the simulation program.

<sup>a)</sup>Author to whom correspondence should be addressed; electronic mail: phil.turner@sira.co.uk

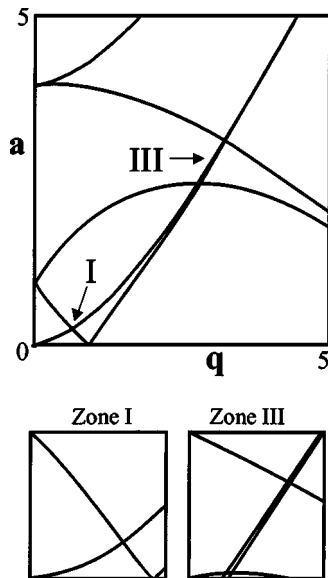


FIG. 2. Mathieu stability diagram showing zones I and III.

$$a_u = a_x = -a_y = \frac{4eU}{m\omega^2 r_0^2},$$

$$q_u = q_x = -q_y = \frac{2eV}{m\omega^2 r_0^2},$$

where  $V$  is zero to peak rf,  $U$  is the dc voltage,  $e$  is the electronic charge,  $\omega$  is the angular frequency of the rf voltage, and  $r_0$  is the inner radius of the quadrupole. Where the  $x$  and  $y$  stable regions coincide, stable trajectories through the analyzer are possible, allowing successful transmission. Throughout the literature, each stability region where the  $x$  and  $y$  stability overlap has been referred to under a number of different terms. Here, the notation as given by the early work of Dawson and Bingqi is used.<sup>7</sup>

Most commercial instruments use zone I, the tip of the stability region giving the maximum resolution ( $a=0.23, q=0.71$ ) other zones, however, can also be used to produce mass spectra. The zone III region is rectangular in shape and resolution can be obtained at the upper ( $a=3.16, q=3.23$ ) or lower tip ( $a=2.52, q=2.82$ ) of zone III, as shown in Fig. 2 (bottom right).<sup>8</sup>

Peak shapes in zone III are generally better resolved than if zone I is used. However, the mass range is limited because much higher operating voltages are required, and this has discouraged its use. Zone III quadrupoles have been applied in a number of applications, including resolving  $\text{CO}^+$  and  $\text{N}_2^+$ ; hydrogen, helium, and deuterium studies; and also in resolving  $\text{CH}_3^+$  and  $^{15}\text{N}^+$ .<sup>9-11</sup>

## II. SIMULATION RESULTS

The initial focus of the work was to look at the initial position in the  $x$ - $y$  plane of those ions that successfully reach

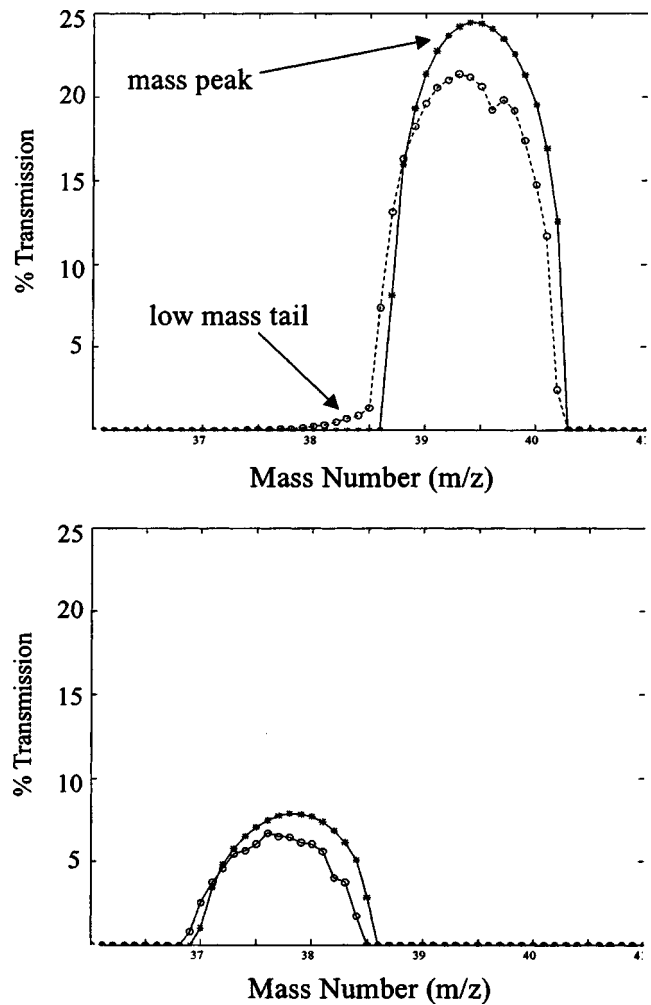


FIG. 3.  $10^6 \text{Ar}^+$  ions ( $m/z=40$ ) are emitted from the source. Number of successfully transmitted ions for round electrodes (\*) and hyperbolic electrodes (o) for both zones I (top) and III (bottom) are shown.

the detector. Results for such studies exist for the hyperbolic electrodes for the first stability region. This work examines the behavior for round rods.

Previous computations<sup>2</sup> for zone I show changes in ion origin progressing along the mass scale from the lower mass side to the upper mass side of the peak. Here, quadrupole conditions have been chosen to match previous work. Quadrupole parameters are as follows: Length=127 mm, radius,  $r_0=2.768$  mm, and  $f=4$  MHz with an ion energy of 2 eV and  $r/r_0=1.148$ .  $10^6$  ions of  $\text{Ar}^+(m/z=40)$  will be simulated at each mass point.

Figure 3 (top) are computer simulations of a zone I quadrupole for both hyperbolic and circular electrodes. When employing circular electrodes it is well-known that the performance of quadrupole instruments is adversely affected. It can be seen that a long low-mass-side tail is produced. However, circular electrodes are employed as they are less expensive to produce. This has previously been demonstrated by computer simulation<sup>3</sup>.

Figure 3 (bottom) shows the results for using the third stability region, with the same number of ions emitted from

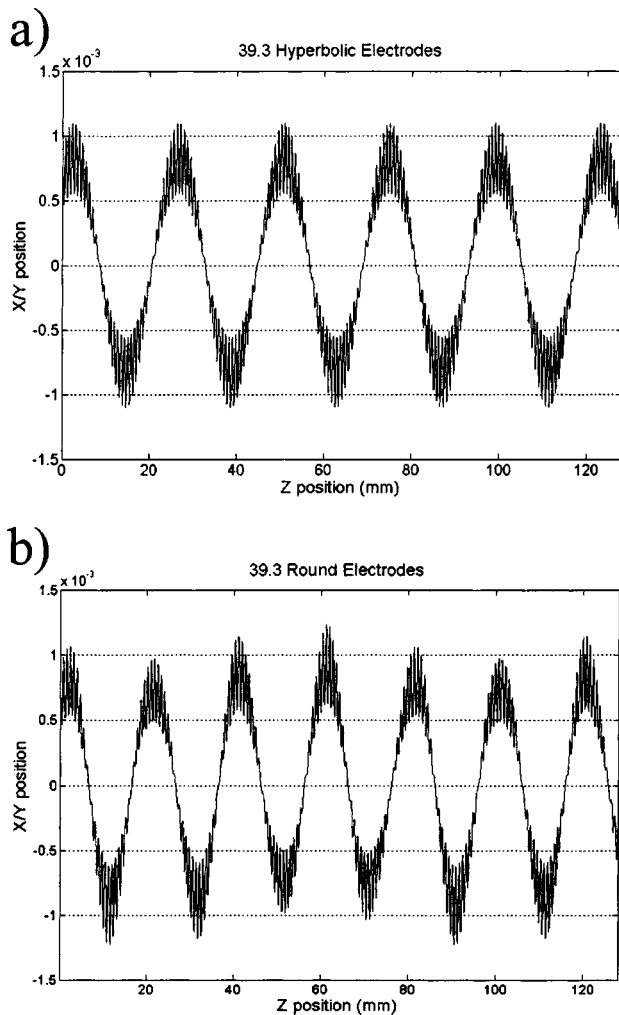


FIG. 4. Ion trajectories for zone I in the  $x$  direction for (a) hyperbolic and (b) round rod electrodes.

the ion source. The sensitivity is greatly reduced, and the peak appears shifted down the mass scale. There is no low-mass tail for zone III, and peak shape is more regular when using hyperbolic rods in both regions.

### A. Ion trajectories

In Fig. 4(a), the ion trajectories for motion in the  $x$  direction are shown for zone I for hyperbolic electrodes. These are comparable with those plotted by Dawson<sup>12</sup> and provide further model validation. In Fig. 4(b), the trajectories for motion in the direction are shown for zone I for round electrodes.

Although the general features are the same there are subtle differences for an ion injected at the peak of the mass spectrum for zone I. The same  $x$ - $y$  position, ion energy and phase for hyperbolic and round electrodes were used. The amplitude variation of ion trajectories is greater in the round rod case, and the frequency of oscillation is also different. This is due to slight differences in the electric field provided by the electrode systems.

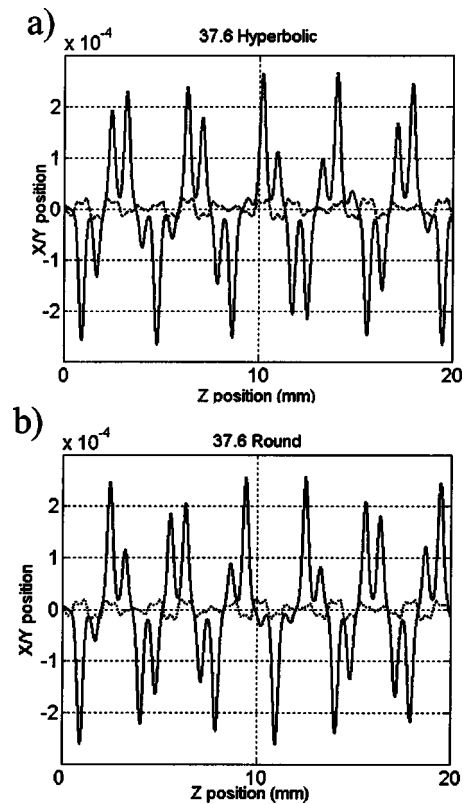


FIG. 5. Ion trajectories for zone III in both  $x$  and  $y$  directions for (a) hyperbolic and (b) round rod electrodes.

In Fig. 5(a) and 5(b) show the ion trajectories for an ion injected at the peak of the mass spectrum for zone III. Using the same conditions for hyperbolic and round electrodes. Motion in the  $x$  and  $y$  directions are shown.

Noteworthy is the large difference in the form for trajectories for zones I and III stability regions. Ion oscillations in zone III are more sinusoidal compared to those in zone I. Furthermore, the amplitude of the ion oscillation in the  $x$  and  $y$  directions is approximately one order of magnitude lower in the case of zone III ions compared to zone I.

Ion trajectories will also correspond to the Mathieu stability diagram. Zone III has a narrow  $x$  stable region and, therefore, motion in the  $x$  direction will be small for a successful ion.

### B. Ion origin

Figure 6 shows a contour plot ( $>500$  ions) for ion origin for round electrodes, indicating changes in the shape of the ion source region. That permits the successful transmission of ions through the analyzer. The  $x$ - $y$  cross section was split into a grid. The number of ions at each grid point was summed, and the contour here shows regions  $>500$  ions. This corresponds to 0.2% peak height, emphasizing features in the low-mass tail. In Fig. 6 ( $m/z=38.2$ ), Those ions responsible for the low-mass tail are shown to be two points along the  $x$  axis. The low-mass tail intensity increases as  $m/z$  increases. The ion origins can be seen in greater detail in Fig. 7 as a series of three-dimensional (3D) contour plots.

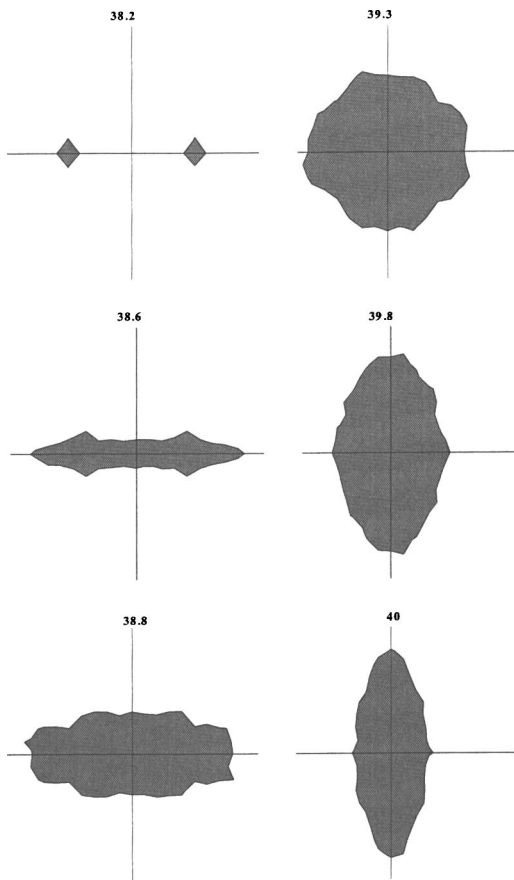


FIG. 6. Contour plots indicating regions of ion origin for a round-electrode quadrupole mass spectrometer operated in the first stability region. Mass-to-charge ( $m/z$ ) ratios are shown to indicate peak position (Fig. 3).

Figure 7 shows two peaks on the  $x$  axis on either side of the center that increases in magnitude with  $m/z$  value until the body of the main peak is reached. Eventually, space between them fills, producing a single elongated peak that broadens to be circular when approaching maximum transmission. The diagrams correspond to the same simulation used for Fig. 3 and the contour maps in Fig. 6.

The region on the  $x$ - $y$  entrance plane for these ions responsible for the low-mass tail is identified. In all other respects, ion origin characteristics for the round rods, match those for the hyperbolic rod set in zone I. As shown in Fig. 6 in the low-mass side of the peak, the majority of ions originate on or along the  $x$  axis. At the peak, ions originate from a uniform disc about the central axis, at the high mass side of the peak and ion origin is from the  $y$  axis.

Figure 8 shows the corresponding contour plot, but for zone III operation. The results are shown for round electrodes, in this zone, little difference is seen between hyperbolic and round electrodes. However, 500 ions will represent a greater percentage of the peak than in Fig. 6 because of the reduced sensitivity of zone III. The 500 ions correspond to 0.5% peak height. Throughout the peak, ions all originate on the  $x$  axis. This is expected, when the  $x$  and  $y$  stable regions in the Mathieu stability diagram for zone III are examined.

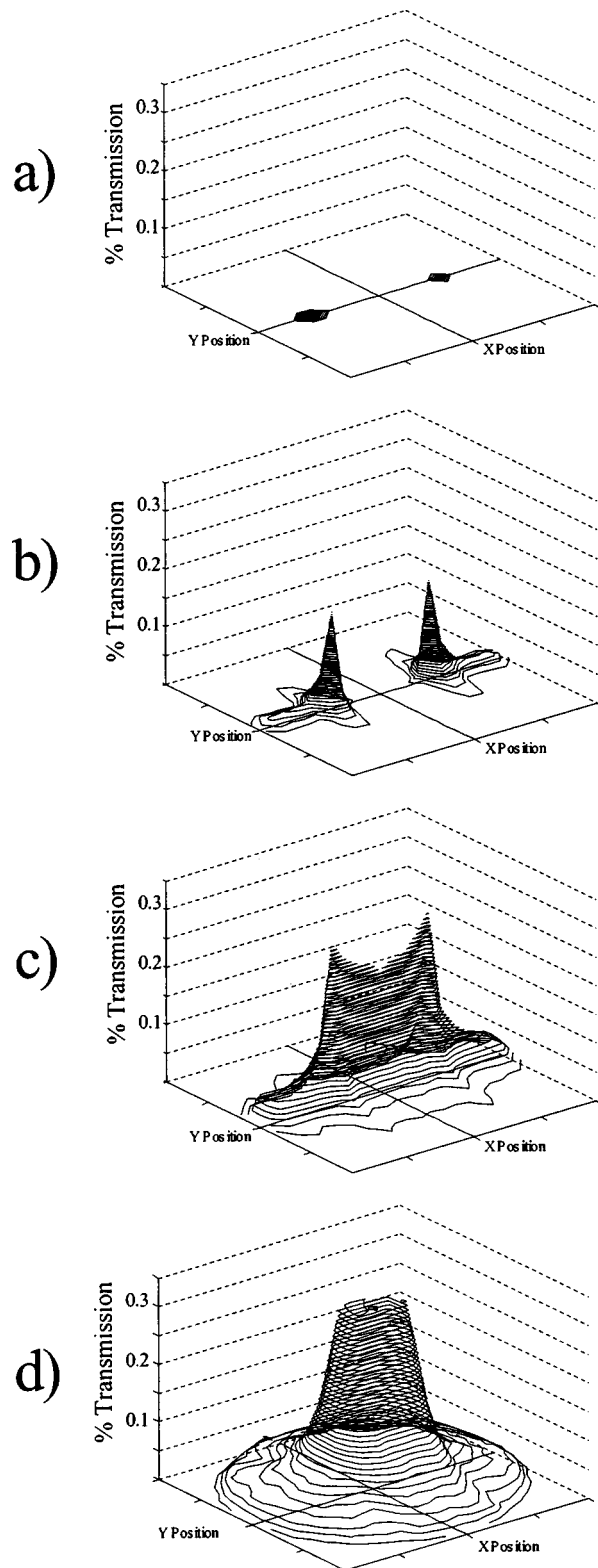


FIG. 7. 3D contour plots of ion origin with increasing  $m/z$  value. Focusing on the low mass tail region  $m/z=37.5$  (a),  $m/z=38.5$  (b),  $m/z=38.6$  (c), and  $m/z=39.3$  (d).

This zone is narrow in shape due to the narrow  $x$  stable region; any transmitted ions must remain in this narrow  $x$  stable band.

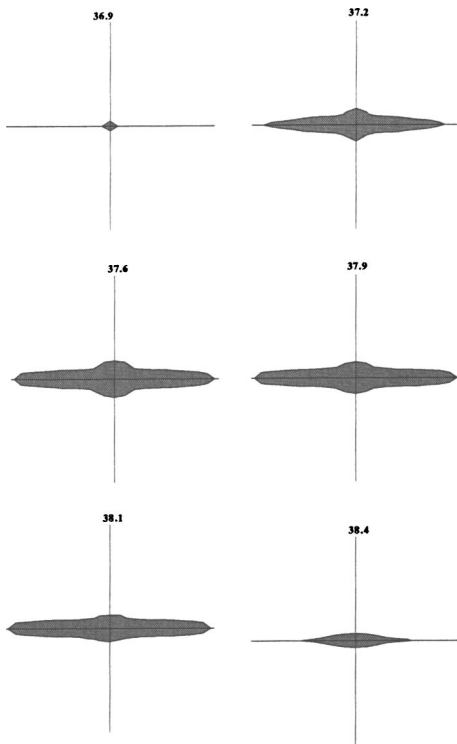


FIG. 8. Contour plots indicating regions of ion origin for round electrodes for a quadrupole mass spectrometer operated in zone III of the Mathieu stability diagram.

For zone III, the loss of sensitivity could be improved by the ion source focusing ions onto the  $x$  axis. Increasing the number of ions entering the quadrupole in this region would increase transmission probability. According to the results of Fig. 8 any ions entering off the  $x$  axis are rejected.

### C. Ion transmission and phase angle

Another factor that alters the transmission probability of an ion through the quadrupole is the phase of the rf cycle as the ion enters the quadrupole rods. Figure 9 shows plots of  $x$  and  $y$  position with phase angle for round rods in the first stability region and emphasizes how the  $xy$  acceptance positions depend on the phase angle. This is related to the previous zone I (Figs. 2–4), and again, the exchange from  $x$  axis to  $y$  axis transmission can be seen across the peak with increasing mass.

In Fig. 3, mass 39.5 can be regarded as the peak maximum, with successful ions being transmitted from all areas of the ion source. Figure 9 shows that the area of transmission is at a maximum when the phase angle is equal to  $\pi$ . Importantly, Fig. 9 shows that in the low-mass tail, no ions are transmitted at a phase angle of  $\pi$ . The  $x$  acceptance position changes with phase. This can be considered as a band, with the low-mass-tail ions originating along the parameter of this band. At a phase angle of  $\pi$ , no transmission of ions occurs in the low-mass tail. The “real” peak occurs at the point when the area between the parameter bands is filled, also corresponding to  $m/z=38.6$  in Figs. 5 and 7. The width of the  $x$  transmission band then continues to narrow with

increasing  $m/z$  value.  $y$  axis ion transmission also exhibits changes; again, no  $\pi$ -transmission is emphasized. The area of transmitted ions gradually increases from the low-mass side to the high-mass side.

Figure 10 shows ion transmission and the effect of the phase angle for the zone III stability region. As already shown in Fig. 8, transmission is along the  $x$  axis, as expected. It is immediately seen that there are very significant differences. For zone III at a phase angle of about  $3/5\pi$  and  $7/5\pi$  the ions are being transmitted along the entire  $x$  axis. 0 and  $2\pi$  ions also show a wider area of origin. This is in contrast to the first stability region ignoring the low-mass tail, where transmission across the entire  $x$  axis occurs at an angle of  $\pi$ .

Figure 11 sums, at each mass step of the simulation, the number of successful ions at each phase angle. The first region (top) indicates that the largest numbers of ions are transmitted at a phase angle of  $\pi$ . The low-mass tail has no  $\pi$ -originating ions. The zone III region Fig. 11 (bottom) indicates that the majority of the ions are transmitted at phase angles of 0 and  $2\pi$ , with the features in Fig. 11 at about  $3/5$  and  $7/5\pi$  having a minor contribution.

## III. DISCUSSION

Given this information, if the ion source was pulsed and synchronized with the rf phase such that ions only entered the quadrupole analyzer at a phase angle of  $\pi$  or close to it, the low mass tail would effectively be removed.

Figure 3 show that the presence of a low mass tail will give incorrect readings for nearby preceding peaks. The low-mass tail can be up to 5%–10% of the peak height. Phase filtering by pulsing the ion source will reduce the sensitivity of the instrument, but given substantially corrects this feature of round electrode quadrupoles.

Figure 12 investigates the resultant effects on the original peak by employing a phase filter. Here simulations were repeated to give a mass-scale resolution of 0.05 compared to 0.1  $m/z$ . For each transmitted ion the phase angle is known. Ions entering the quadrupole outside the limits of the phase filter can then be removed by subtracting the ions contribution to the transmission values. Figure 12 (left) shows the low-mass tail magnified for clarity.

The sensitivity is reduced as the filter narrows. There is an optimum filter width, which is found to be around  $\pi \pm \pi/8$ . This corresponds to the width of no ion transmission as in Fig. 10 ( $m/z=38.5$ ). Beyond this, the low-mass tail is found to decrease at a similar rate to the sensitivity such that there is no advantage.

In Fig. 12, at mass 38.5, it is found that a  $\pi \pm \pi/8$  filter gives about a 90% reduction in the low-mass tail at the expense of a 50% reduction in sensitivity. A wider filter  $\pi \pm \pi/2$  gives a 50% reduction in low-mass tail at a 30% reduction in sensitivity. The original low-mass tail at this mass was about one-tenth of the peak height. Such features may lead to large inaccuracies in determining minor constituents and isotopes, and they adversely affect instrument resolution.

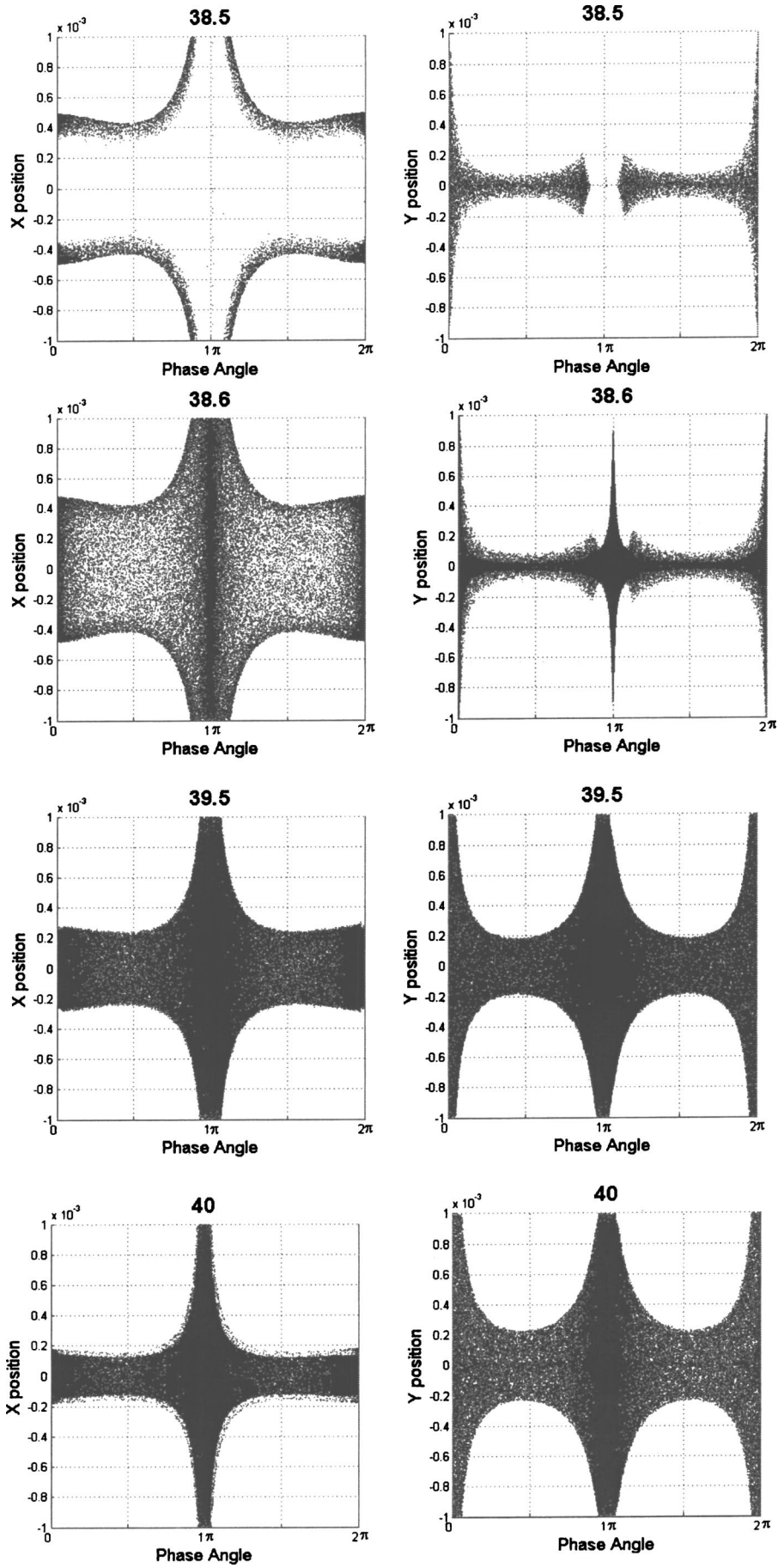


FIG. 9. Changes in x transmission regions of the ion source with phase angle for zone I using round electrodes.

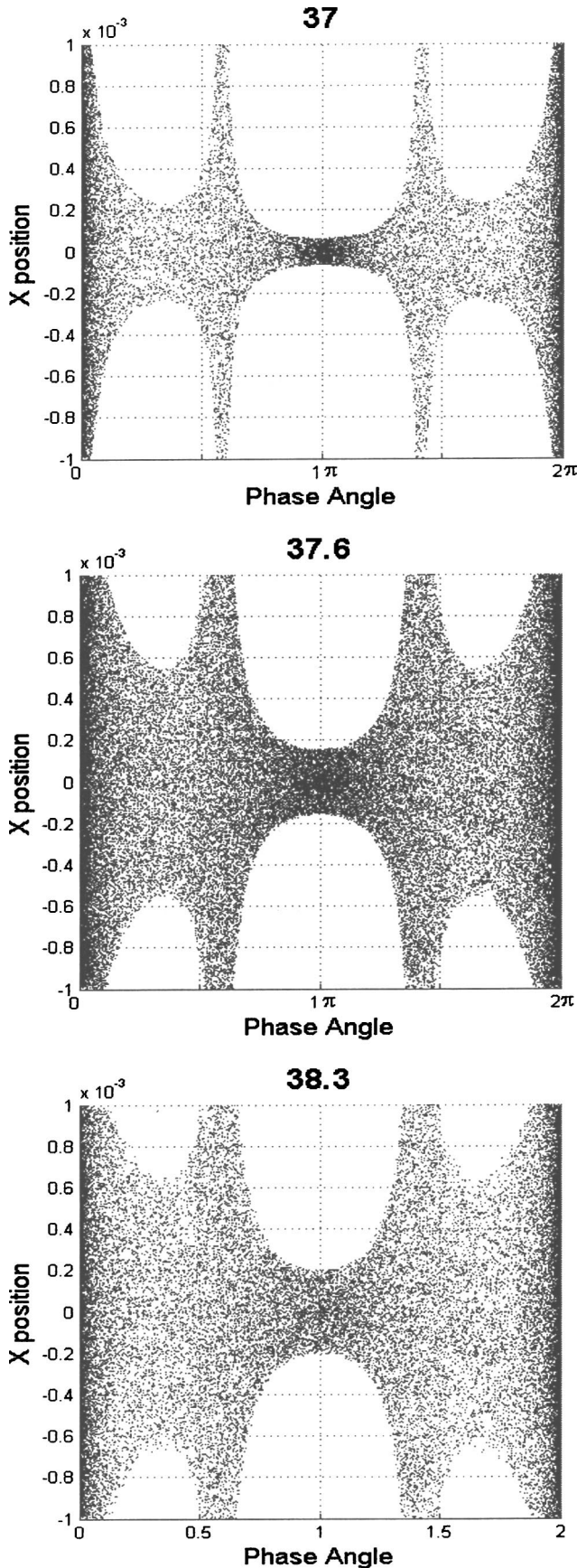


FIG. 10. Changes in  $x$  transmission regions with phase angle for zone III using the round electrodes.

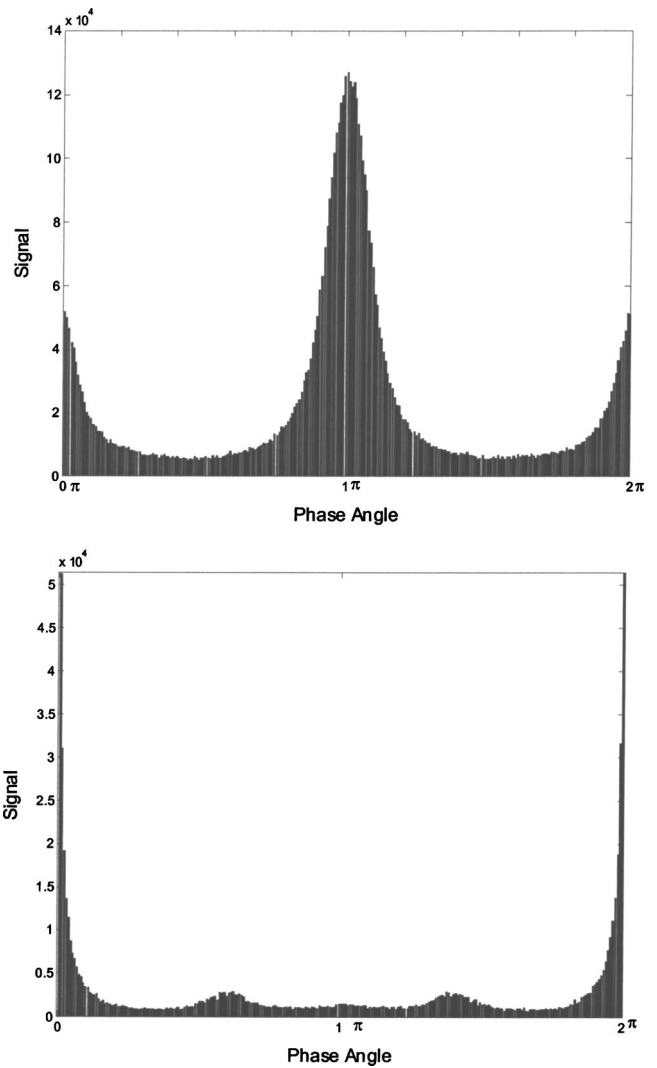


FIG. 11. Summation of transmitted ions with phase angle across an entire mass peak.

#### IV. CONCLUSIONS

Computer simulation investigating both round and hyperbolic electrodes has been used to study ion origin for stability zones I and III. There is a shift in the mass at which peak transmission occurs in the case of a quadrupole mass spectrometer operated in zone III. Mass spectrometers are tuned to a mass defined by an external standard, so this is easily corrected. Ion trajectories have been shown for the cases of hyperbolic and round electrodes for both stability regions. The form of the ion trajectories in the case of stable ions transmitted at the zone III region of operation is, in general, very different from those transmitted in zone I. The program allows detailed study of these effects.

The ion-source transmission regions for zones I and III have been established. This could have relevance to instrumental development regarding the ion source. If the ion-source exit aperture were to have a cross-hair design, ions would not be able to reach the detector on axis. The number of ions on the high- and low-mass side of the peak would be reduced, sharpening the peak and increasing resolution at a

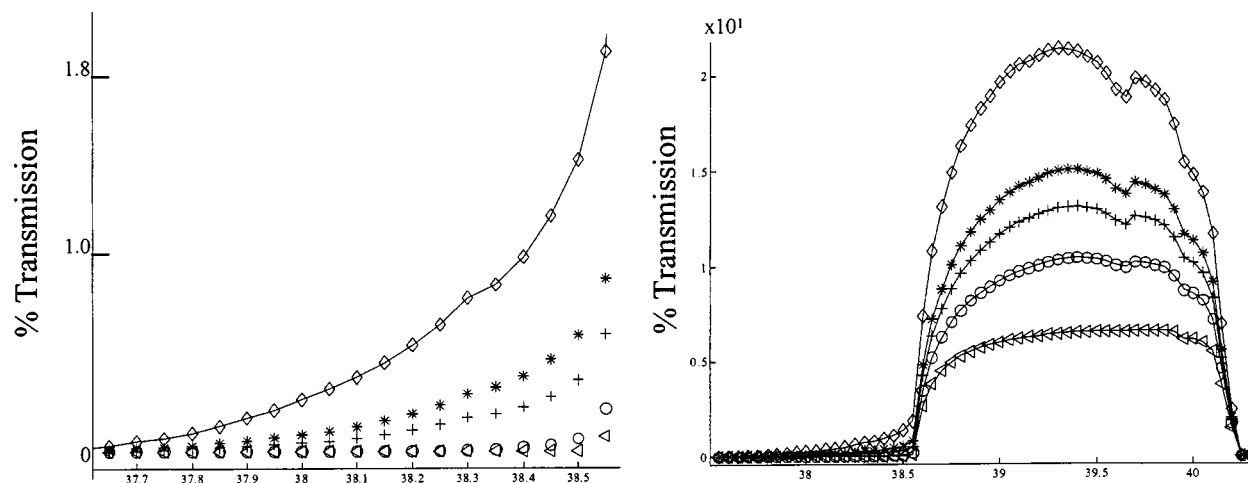


FIG. 12. Effect of employing a pulsed ion source to control the phase angle at which the ions enter the quadrupole analyzer. Different pulses are shown corresponding to no filter ( $\diamond$ ), then  $\pi \pm \pi/2$  (\*),  $\pi \pm \pi/4$  (+),  $\pi \pm \pi/8$  (o), and  $\pi \pm \pi/16$  ( $\Delta$ ).

cost of sensitivity. However, precision production methods would have to be employed to ensure correct alignment and that the reduction in sensitivity is within reasonable boundaries.

Causes of the low-mass tail seen when using round rods have been found to depend upon the rf phase at the point of ion entry. Pulsing the ion source has been suggested and evaluated by simulation as a method of low-mass-tail correction.

## ACKNOWLEDGMENTS

We are grateful to Sira Ltd for their support, to Professor Harry Leck for his help and advice, and to the EPSRC industrial case Studentship allocated by the Intersect Faraday Partnership.

<sup>1</sup>P. E. Miller and M. B. Denton, *J. Chem. Educ.* **63**, 7 (1986).

<sup>2</sup>J. R. Gibson and S. Taylor and J. H. Leck, *J. Vac. Sci. Technol. A* **18**, 237 (2000).

<sup>3</sup>J. R. Gibson and S. Taylor, *Rapid Commun. Mass Spectrom.* **14**, 1669 (2000).

<sup>4</sup>J. R. Gibson and S. Taylor, *Rapid Commun. Mass Spectrom.* **15**, 1960 (2001).

<sup>5</sup>J. R. Gibson and S. Taylor, *Rapid Commun. Mass Spectrom.* **17**, 1051 (2003).

<sup>6</sup>J. J. Tunstall, S. Taylor, A. Vourdas, J. H. Leck, and J. Batey, *Vacuum* **53**, 211 (1999).

<sup>7</sup>P. H. Dawson and Y. U. Bingqi, *Int. J. Mass Spectrom. Ion Processes* **56**, 25 (1984).

<sup>8</sup>N. V. Konenkov and V. I. Kratenko, *Int. J. Mass Spectrom. Ion Processes* **108**, 115 (1991).

<sup>9</sup>Ma'an H. Amad and R. S. Houk, *J. Am. Soc. Mass Spectrom.* **11**, 407 (2000).

<sup>10</sup>S. Hiroki, T. Abe, and Y. Murakami, *Rev. Sci. Instrum.* **62**, 2121 (1991).

<sup>11</sup>K. Kaneko, S. Hiroki, T. Abe, and Y. Murakami, *Vacuum* **47**, 1313 (1996).

<sup>12</sup>P. H. Dawson, *Quadrupole Mass Spectrometry and its Applications* (Elsevier, New York, 1976), p. 35.